CLM-P786

CLM-P786

UKAEA

Preprint

HIGH TEMPERATURE PLASMA MEASUREMENTS USING LASERS

N. J. Peacock

CULHAM LABORATORY
Abingdon Oxfordshire
1986

† HIGH TEMPERATURE PLASMA MEASUREMENTS USING LASERS

N J Peacock
Culham Laboratory, Abingdon, Oxon, OX14 3DB, UK
(UKAEA/Euratom Fusion Association)

Abstract

The development of laser probe techniques for high temperature plasma diagnostics is reviewed and illustrated through references to several important light scattering experiments during the last two decades. Thomson scattering from the probe beam, in principle, provides all the information on the electron and ion motion. In relatively low density plasmas such as exist in tokamaks, the electron feature $S_e(\kappa,\omega)$ of the spectral density function of the scattered light is used to deduce the spatial variation of the electron temperature and density profiles. In higher density plasma the ion feature $S_i(\kappa,\omega)$ is often a more accessible quantity.

Recent research in tokamaks is aimed at spatial information either using complex viewing optics or in the case of large plasma dimensions, LIDAR techniques. As plasmas temperatures reach 10's of keV, relativistic effects play a role. In tokamaks, detection of the electron cyclotron motion is specific in $\underline{\kappa}$ space and has led to the measurement of magnetic field profiles. Techniques for measuring the ion fluctuation spectrum simultaneously along several $\underline{\kappa}$ vectors are described, with applications to the plasma focus device and to laser produced plasmas. Finally, non-linear resonant wave mixing is proposed as a method for enhancing the density fluctuations and hence the scattered light signal.

August 1986

† Paper presented to

Second Tropical College on Applied Physics: Laser and Plasma Technology (Kuala Lumpur - Malaysia, 17th March - 5th April 1986).

1. INTRODUCTION

The passage of a diagnostic light beam through a plasma is weakly attenuated by photon scattering from the free electrons, ie, Thomson scattering. The first practical demonstration of Thomson scattering was made on an electron beam with a density $n_e \sim 5 \times 10^9$ cm^{-3}, Fiocco and Thomson (1963,a), and not, as is now more usual, on the electrons in a plasma. However, plasma applications followed quickly eg Fiocco and Thomson (1963,b), and an account of these early developments in Thomson scattering is given by Evans and Katzenstein (1969). As we shall demonstrate, the scattered light amplitude is proportional to the level of the electron density fluctuations which may be due, in the simplest case, to their thermal motion. In the more complicated general case, light is scattered by the individual electrons plus their collective motion, the collective density fluctuations arising from ion thermal motion, or from the many different types of waves, resonances and turbulence into which the free energy of the plasma can be channelled.

In this first part of the paper, a concise and simple introduction to the interpretation of Thomson scattering is given. The subsequent account of plasma scattering experiments is included as an illustration of the wide range of topical applications of this diagnostic method.

We should note that Thomson scattering has a wide range of applicability in the study of laboratory plasmas. The electron density can be low as $n_e \sim 10^{10}$cm^{-3} or as high as $n_e \sim 10^{22}$ cm^{-3}, these approximate limits being set by photon statistics at the low end and by laser transmission cut-off at the highest densities. Plasma temperatures ranging from $T_e \sim$ 1eV to $T_e \sim$ 10 keV have been investigated. Transient plasmas with sub-nanosec life times can be probed successfully using laser pulses with appropriately short duration. In other experiments on long-lived plasmas, the uniquely high brightness of pulsed laser probe beams is often essential to scatter sufficient light above the background emission.

2. THE INTERPRETATION OF THE SCATTERED LIGHT SPECTRUM

- General Principles

For reviews of light scattering as applied to plasma diagnostics the reader is referred to articles such Evans & Katzenstein (1969) and Sheffield (1975). The following treatment is a much simplified account of the problem.

The scattering cross-section for a single electron can be calculated from the radiated energy due to the jitter of the electron, imposed by the field of the laser beam, as a fraction of the incident Poynting flux. We consider a polarised wave field which imposes a jitter velocity to the electron in phase with the incident light frequency and which is given by

$$\tilde{v} = \frac{eE_L}{m\omega_0}$$

The ratio of the radiated power to incident flux is given by

$$\frac{\frac{d\varepsilon}{dt},}{I_{inc}} = \frac{\frac{2}{3}\frac{e^2}{c^3}\left(\frac{e\tilde{E}}{m}\right)^2}{\tilde{E}^2\, c/4\pi} = \frac{8}{3}\pi\left(\frac{e^2}{mc^2}\right) = \frac{8}{3}\pi r_e^{\,2} = \sigma_T \qquad (1)$$

$$= 6.65 \times 10^{-25}\ \text{cm}^2$$

The scattering cross-section σ_T is seen to be independent of ω_0 and proportional to $\frac{1}{m^2}$. Thus the electrons are the only effective scattering particles in a plasma. Their radiation pattern is characteristic of a dipole, Fig 1, with a differential cross-section

$$\frac{d\sigma}{d\Omega} = r_e^{\,2} \sin^2\phi$$

The frequency shift seen by an observer of the scattered radiation along the vector $\underline{\kappa}_s$, Fig 1, due to the two stage Doppler effect of the moving electron $\underline{v}$ is given by

$$\Delta\omega = \omega_s - \omega_0 = (\underline{\kappa}_s - \underline{\kappa}_0).\ \underline{v} = \underline{\kappa}.\underline{v} = \left|2\frac{\omega_0}{c}\sin\theta_{/2}\ v\right| \qquad (2)$$

Thus, velocity vectors $\underline{v}$, are sampled by the observer along $\underline{\kappa}$ only, where $\underline{\kappa}$ is the differential scattering vector, whose magnitude is

$$|\underline{\kappa}| = 2|\kappa_0|\ \sin(\theta/2) \qquad (3)$$

A uniform distribution of electrons which can be considered to lie in planes separated by $2\pi\kappa^{-1}$ would lead however to exact cancellation of the electric field associated with the scattered radiation at the detector. In reality random statistical density fluctuations $\tilde{n}_e$ ensure that the difference in the populations of equal volume elements in the plasma scales as $n_e^{\frac{1}{2}}$ and this results in a scattered light intensity at

the detector P_s proportional to $|\tilde{n}_e|^2$ ie to n_e. In an ensemble of electrons, as in a plasma each electron contributed its own Doppler shift to the scattered light spectrum. If $S(\kappa,\omega)$ is the shape factor of the scattered light spectrum then

$$\sigma(\underline{\kappa},w) = \frac{3}{8\pi}\,\sigma_T\, S(\underline{\kappa},\omega)$$

$S(\kappa,w)$ represents the level and spectrum of the electron density fluctuations in the plasma, and is related to $\tilde{n}_e$ by

$$\frac{\tilde{n}_e}{n_e} = \left(\int \frac{d^3\underline{\kappa}}{(2\pi)^3}\,\frac{S(\underline{\kappa},\omega)}{n_e}\right)^{\frac{1}{2}}$$

where the integration is taken over all $\underline{\kappa}$ space.

The actual fluctuation level has been worked out by Evans et al (1983), Pots et al (1981) for a thermal plasma.

With the assumptions that

(i) Observation time $\tau \gg 1/\omega_0$.

(ii) Electron velocities are random (thermal)

(iii) Wave field does not perturb plasma ie

$\tilde{v} < v_e$, where v_e is the mean thermal electron velocity.

(iv) Electron velocities are non relativistic, $v/c < 1$ (ie σ_{scat} indep of ω_0)

then, the scattered spectrum is a Gaussian with a 'form factor' viz,

$$S(\kappa,\omega) = \left(\frac{1}{\pi^{\frac{1}{2}}\,\kappa\, v_e}\right) \exp - \{(\omega-\omega_0)/\kappa v_e\}^2 \qquad (4)$$

$$\Delta\lambda_{FWHM} = 4\lambda_0 \,\mathrm{Sin}\,(\theta/2)\left[2k\,\frac{T_e}{m_e c^2}\,\ell n 2\right]^{\frac{1}{2}} \qquad (5)$$

The scattered power received at a point R from an irradiated volume, V, is given by

$$P_{scat}(R,\omega_s)\ d\Omega = P_{inc}\ n_e \frac{d\sigma}{d\Omega}\ d\Omega.L.S(\kappa,\omega) \qquad (6)$$

$$= P_{inc}\ n_e r_e^2 (1-\sin^2\theta.\cos^2\phi)\ d\omega.V.S(\kappa,\omega)$$

with $r_e^2 = 2.95 \times 10^{-26}\ cm^{-2}$ and for typical experimental values of the irradiated plasma length L, viewed at R, and a collection solid angle $d\Omega$ etc then,

$$\frac{P_{scat}}{P_{inc}} \sim 10^{-12} \rightarrow 10^{-15}$$

, hence the need for laser light intensities.

The assumption above are now considered more closely. The first assumption is automatically satisfied with visible or FIR probe beams. We will discuss the second assumption, ie., that pertaining to the velocity distribution of the electrons, throughout the text. The third assumption, that there is no heat deposition into the plasma from the probe beam, can readily be calculated to hold good provided that the probe frequency remains greater than the electron plasma frequency, $\omega_{pe} = \left(\frac{4\pi n_e e^2}{m_e}\right)^{\frac{1}{2}}$. The increase in temperature of a hydrogen plasma due to frictional collisions in the laser beam of cross section A_0 for example, is given by

$$\frac{\Delta T_e}{T_e} = 3.6 \times 10^{-17} \frac{\lambda 2\ n_i}{A_0} \frac{\ell n\ \Lambda}{T_e^{5/2}} \int_0^{\tau} P_0\ dt$$

where P_0 is the incident laser power. At $n_i = n_e = 1 \times 10^{19}\ cm^{-3}$ and $T_e \sim 300$ eV, $\ell n\Lambda = 9.0$ ($\Lambda = 12\ n_e \lambda_D^3$ where λ_D is the Debye screening distance), and with $\int P d_0.dt = 6j$ and $A_0 = 1\ cm^2$, then $\Delta T_e/T_e \sim 6 \times 10^{-5}$.

The fourth assumption breaks down for near relativistic electron velocities were $h\nu \sim mc^2$. In this case discussed by Sheffield (1975) and Selden (1980), the scattering cross section is no longer independent of ω_0. The radiation, moreover, is no longer dipole but exhibits a temperature- dependent blue shift with associated polarisation changes. The incident light is scattered preferentially in the forward $\beta = (v/c)$ direction figure 2, with a change in wavelength (the Compton shift) given by $\Delta\lambda = \frac{2h}{mc} \sin(\theta/2)$. At relativistic speeds the cross-section is given by the Klein-Nishina formula, Sheffield (1975). Figure 3 illustrates the progressive shift

of a Maxwellian distribution as the plasma temperature is raised from 0.5→50 keV. The plot, Selden (1982), relates the form factor

$$S_e\left[\frac{\omega_0 - \omega_s}{\omega_s},\ \theta = 90°\right] \text{ to the normalised wavelength shift } \left[\frac{\omega_0 - \omega_s}{\omega_s}\right].$$

We have seen that the dynamic form factor $S(\kappa,\omega)$ presents the spectrum of light scattered from uncorrelated motion in an ensemble of electrons. This is only a limiting case applicable to $(\underline{\kappa}\ \lambda_D)^{-1} << 1$ ie to small scale fluctuations of the electron density. In the general case $S(\kappa,\omega)$ contains information on both random and correlated motions of the electrons. The spectrum over all ω is the temporal Fourier transform of all the density fluctuations whose spatial scale length is κ^{-1}. Some of the spatial Fourier components are natural plasma modes and electron density fluctuations due to ion motion will only occur at $(\kappa\lambda_D)^{-1} \tilde{>} 1$ ie for scale lengths of the order of or exceeding the Debye length λ_D. $(\kappa\lambda_D)^{-1}$ is often termed the 'scattering parameter', α, where

$$\alpha = \frac{1.08 \times 10^{-4}}{\sin\theta/2}\ \lambda\ \left(\frac{n_e}{T_e}\right)^{\frac{1}{2}}, \text{ with } \lambda \text{ in cm, } n_e \text{ in cm}^{-3} \text{ and } T_e \text{ in eV.} \qquad (7)$$

There is an intimate relation between the scattered light spectrum, when selecting a given $\underline{\kappa}$ vector, and the dispersion relation for plasma waves. As illustrated in Fig 4 the dispersion relation gives the frequencies at which the peaks will occur.

For the Langmuir waves, for example, we have the Bohm-Gross relation (valid for $\lambda > \lambda_D$).

$$\omega_0^2 = \omega_{pe}^2 + 3\left(\frac{kT_e}{m}\right)\kappa^2, \text{ where } \omega_{pe} \text{ is the plasma frequency.} \qquad (8)$$

$S(\kappa,\omega)$ not only contains the position of the resonances but carries information also on the strength of the fluctuations at all frequencies and therefore on the intensities to which the waves have developed.

3. ELECTRON AND ION COMPONENTS OF THE SCATTERED LIGHT SPECTRUM

In the following, $S(\kappa,\omega)$ is discussed in terms of the electron and ion susceptibilities G_e and G_i where the plasma longitudinal dielectric constant is

$$\varepsilon = 1 - G_e - G_i$$

$$S(\kappa,\omega) = \frac{|1 - G_i|^2 f(v_e) + Z|G_e|^2 f(v_i)}{|\varepsilon|^2} \qquad (9)$$

, where $G_e = -\alpha^2 W$ and $G_i = -Z\,(T_e/T_i)\,\alpha^2 W$ are the dielectric susceptibilities. W is the plasma dispersion function, Fried and S D Conte (1961), and $f(v_e)$, $f(v_i)$ are the electron and ion velocity distributions respectively.

The first and second terms contribute two distinct features to the spectrum $S(\kappa,\omega)$ Fig 5, and are often called the electron and ion components, respectively.

For $\alpha \ll 1$ G_i, G_e can be neglected and we recover $S(\kappa,\omega) = f(v_e)$, ie the spectrum due to the uncorrelated thermal motion of the electrons.

For $\alpha > 1$ G_i, G_e no longer vanish and the ion term dominates for low frequency shifts, $\Delta\omega \sim \kappa v_i$

$$S(\kappa,\omega) = \frac{2\pi^{\frac{1}{2}}}{\kappa v_e} \Gamma_\alpha\,(x_e) + \frac{2\pi^{\frac{1}{2}}}{\kappa v_i} Z\,\left(\frac{\alpha^2}{1+\alpha^2}\right)^2 \Gamma_\beta(x_i), \qquad (10)$$

, where $\Gamma_\alpha = [1 + \alpha^2\,\mathrm{Re}[W(x)]]^2 + [\alpha^2 \mathrm{Im}[W(x)]]^2$,

$$\beta = \frac{Z\alpha^2}{1+\alpha^2}\,\frac{T_e}{T_i} \qquad (11)$$

$$x_{e,i} = \omega/\kappa v_{e,i}$$

where $v_{e,i}$ are the thermal velocities of the plasma components.

The above expression for $S(\kappa,\omega)$ is valid in the Saltpeter approximation, Sheffield (1975), ie where the electron and ion temperatures are not very different, $\frac{T_e}{T_i} < 1$, and where, $\beta^2 < 3.45$. In this case we have a narrow central ion feature with $\Delta\omega \sim \kappa v_i$ superimposed on a wide, low electron feature with $\Delta\omega \sim \kappa v_e$.

The form of the spectral distributions for the electrons $\Gamma_\alpha(x)$ and for the ions $\Gamma_\beta(x)$ are similar and are as illustrated in Fig 6.

ELECTRON TERM

For $\alpha << 1$ the ion term is virtually absent and the Gaussian spectral function is determined by the electron velocity distribution. Above $\alpha=1$, the collective effects of the electrons are apparent. The Gaussian shape becomes distorted and the maximum shifts away from zero as α increases above unity. For $1 < \alpha < 2$ the maximum approximately coincides with the numerical value of α. The spectral shift of the maximum is $\sim \sqrt{2}.\omega_{pe}$ and is therefore a measure of the electron density.

ION TERM

For $\alpha \sim 1$ and for $\beta < 0.5$ say, with $T_e \sim T_i$ the ion term is analogous to the electron term and is a Gaussian with width $\Delta\omega = \kappa v_i$, being a measure of the ion temperature T_i. For large α, the β parameter approaches $\beta^2 = T_e/T_i$ and it is this parameter which determines the shape of the spectrum. Ion features measured on the Culham plasma focus illustrate some of these features, Fig 7.

For $1 < \beta < \sqrt{3.5}$ the maximum in the ion spectrum occurs at $\left(\frac{\Delta\omega}{\kappa v_i}\right) = \beta$ ie $\Delta\omega$ (maximum) $= \left(\frac{2\omega^2_{pi}}{1+\alpha^2}\right)^{\frac{1}{2}} = \omega_{pi}$ for $\alpha = 1$ and goes over to ion acoustic waves $\omega_{ac} = \kappa[(Zk\overline{T}_e + 3KT_i)/m_i]^{\frac{1}{2}}$ as α increases. Within the Saltpeter approximation T_e/T_i is restricted to small values $\lesssim 1$, so any ion resonance will be severely Landau damped.

The total scattered light integrated over all frequencies is proportional to $\sigma_T(S_e(\kappa) + S_i(\kappa))$.

The intensity of the scattered light in the electron and ion features are given in Evans and Katzenstein (1969). In the electron component for example, $S_e(\kappa) = \frac{1}{1+\alpha^2}$, and in the ion feature $S_i(\kappa) = \frac{Z\alpha^4}{(1+\alpha^2)^2(1+\beta^2)}$. Thus the total scattering cross section approaches σ_T in the limit $\alpha \to 0$ and is less than σ_T by a factor $Z/(1+ZT_e/T_i)$ as $\alpha \to \infty$.

4. EFFECT OF SUPERIMPOSED ELECTRON DRIFT

When scattering from a plasma which carries a current there is a displacement of the electron velocity distribution relative to the ions. In this case $f(v_e)$ is altered to,

$$f(v_e) = \left(\frac{n_e}{v_e \pi^{\frac{1}{2}}}\right) \exp - \left(\frac{v - \underline{\kappa}\cdot\underline{v}_d}{v_e}\right)^2 \qquad (12)$$

where $\underline{v}_d$ is the electron drift. The electron term $S_e(\kappa,\omega)$ is unchanged except for displacement (usually small) of the Gaussian $\Delta\omega = \underline{\kappa}.\underline{v}_d$. The ion term can be grossly altered however and shows an asymmetry due to enhancement (negative Landau damping) of the ion acoustic wave whose plasma velocity is in the same sense as the drift, with a positive damping on the opposite resonance - see Fig 8.

5. EFFECT OF IMPURITIES

Plasma may contain several ion components. Typically, in fusion research at least, there is a majority species of light ions with a minority of heavier ions present as impurities. Evans (1970) has considered the effect of the higher Z ions on the scattered light spectrum.

In the presence of ions 'j' with susceptibility G_j and velocity distribution $f(v_j)$, the scattering form factor is

$$S(\kappa,\omega) = \frac{|1 - \Sigma G_j|^2 f(v_e) + |G_e|^2 \frac{1}{n_e} \Sigma Z_j^2 N_j f(v_j)}{|1 - G_e - \Sigma G_j|^2} \qquad (13)$$

Modest impurity levels can produce relatively large changes in the ion frequency spectrum and in the scattered light level. This is because the effective ion charge $Z_{eff} = \Sigma Z_j^2 N_j/n_e$ appears explicitly and a small % of highly ionised ions (eg 2% of O^{8+}) can double the effective charge seen by the electrons. An example of the theory compared to experiment has been shown in Figure 7. In this case the neon ion temperature is 9 keV while the principal constituent, deuterium, has $T_i < 1$ keV. Other computed spectral intensities are shown in Fig 9 for oxygen contamination of a high temperature hydrogen plasma.

6. LIGHT SCATTERING FROM A MAGNETISED PLASMA

A general account of the effect of magnetic fields on the scattered light spectrum is given by Sheffield (1975), Carolan (1977), Peacock (1978). Consider light scattered from charged particles performing cycloidal motion about magnetic field lines, Fig 10. Bernstein's theory of plasma waves in a magnetic plasma implies that the scattered light spectrum contains frequency shifts at multiples of ω_{ce}, ω_{ci}.

When sampling density fluctuations along the $\underline{\kappa}$ vectors strictly orthogonal to $\vec{B}$, only the gyrating motion is observable. $\underline{\kappa}$ vectors parallel to $v_\perp$ will therefore see sinusoidally varying Doppler shifts. In the uncorrelated electron spectrum whose width is κv_e, the peaks are spaced out uniformly and separated by ω_{ce}. The envelope to the intensity of the peaks is just the form factor for the electron component, $S_e(\omega,\kappa)$. The depth of modulation to the $S_e(\kappa,\omega)$ envelope has been calculated by Lehner and Pohl (1970).

Rather stringent conditions have to be fulfilled in order that the resonances appear in $S_e(\kappa,\omega)$, viz.,

(i) A condition for the undamped appearance of the resonances is that the orbits should close on themselves within a scale length κ^{-1}. This amounts to a criterion for collisionless orbits, $\omega_{ce}\tau_e >> 1$ ie.

$$\frac{6 \times 10^{12} B T_e^{3/2}}{n_e \ell n \Lambda} >> 1, \text{ with units of Gauss, eV and cm}^{-3}, \quad (14)$$

This criterion is often invalid at high n_e and in turbulent plasma such as the compressed core in the plasma focus where for example the anomalous resistively $\eta_{AN} = 6 \times 10^3 \eta_{spitz}$: $\omega_{ce}\tau_{ee} < 1$: $\omega_{ci}\tau_{ci} \sim 1$, D Muir, PhD Thesis (1983).

(ii) Orbits should close on themselves within the scattered volume ie $2\pi r_L << w$, where w is the width of the laser beam probe.

(iii) There should be multiple phase changes during one gyro period (analogous to scattering from a moving mirror) ie.,

$$\kappa r_L >> 2\pi \quad \text{or} \quad \frac{\bar{\kappa}.v}{\omega_{ce}} >> 1 \quad (15)$$

(iv) No component of $v_\parallel$ to $\underline{B}$, to be accepted ie the misalignment angle 'ε' - see Fig 10 has to be small,

$$\text{ie 'a'} = \left(\frac{\kappa v_\perp}{\omega_{ce}}\right)^2 >> 1, \text{ 'b'} = \left(\frac{\kappa v_\parallel}{\omega_{ce}}\right)^2 << 1 \quad (16)$$

A schematic plot of the modulation to the $S_e(\kappa,\omega)$ envelope is shown in Fig. 11 and illustrates this last criterion. In scattering experiments so far, magnetic modulation has been successfully

demonstrated on a tokamak, Forrest et al (1978), and a θ-pinch, Evans and Carolan, (1970).

7. THOMSON SCATTERING AS A CONSEQUENCE OF REFRACTIVITY

It can be shown, Evans et al (1982), Evans (1984), that Thomson scattering, in common with other optical effects of the free electrons such as phase change interferometry and Faraday rotation, can be considered to result from refraction and diffraction in the plasma medium. In the simplest case considered, that of phase shifts in the transmitted beam due to orthogonally imposed sinsoidal refractive index changes, the resultant intensity distribution at the output lens contains a number of terms. One of these is proportional to the square of the phase change,

$$(\tfrac{1}{2}\Delta\phi)^2 = (\frac{\pi}{\lambda} L\Delta\mu)^2 = \frac{1}{4} r_e^2 \lambda^2 L^2 \tilde{n}_e^2 \qquad (17)$$

which can be recognised as Thomson scattering of a Gaussian beam by a monochromatic electron density wave. The spatial profile of the intensity is given by the same relation as equation (3) describing small angle Bragg scattering.

8. EXAMPLES OF THOMSON SCATTERING DIAGNOSTICS

In this section we describe the use of Thomson scattering as a non-perturbative, time-resolved diagnostic in plasmas of interest in fusion research. A prime example is the history of electron density and temperature measurements in tokamaks using laser beam probes, Section 9. In these relatively low density plasmas, when using visible and near infrared lasers, the scattering parameter α is generally less than unity and the spectral density function, determined by the uncorrelated electron motion, is simply $S_e(\kappa,\omega)$. Information on the internal plasma fluctuations is better illustrated by scattering experiments on higher density plasmas such as the plasma focus and laser-produced plasmas, Sections 11, 12.

9. THOMSON SCATTERING IN TOKAMAKS

In tokamak research, Thomson scattering was first used to measure the spatial electron density and temperature profiles on the T3 tokamak, Peacock et al (1969). The apparatus, relatively unsophisticated by present day standards, is shown in Figure 12. Typical scattered light signals are indicated in Figure 13, while the shape of the Gaussian spectral density functions, Figure 14, have the form of Maxwellian

electron velocity distributions appropriate to the electron temperatures indicated.

Since these early measurements, light scattering apparatus has been modified typically to give continuous or periodic information in time and space during a single discharge. Multiple pulse lasers are often adopted with scattered light collection system which 'view' a substantial part or even the whole of the plasma diameter. The dispersed two dimensional image formed by the spectrometer has spectral information in one dimension and spatial information in the other. Matrix detectors such as silicon intensified targets (SIT's) or charge coupled devices (CCD) are convenient detectors in this type of scattering system see eg Bretz et al (1978), Smith et al (1985). A successful scattering system based on a repetitively pulsed Nd YAG laser has been developed by Rohr et al (1982). This laser system with $\lambda_0 = 1.06\ \mu m$, is capable of operating at 60 Hz for a period of under 7s. The detectors used for the detection of the infrared scattered photons are large sensitive area silicon avalanche diodes. The overall sensitivity of the scattering system is sufficient to measure electron densities as low as $3 \times 10^{12}\ cm^{-3}$. An update of the apparatus and calibration techniques used in Thomson scattering experiments on tokamaks is given by Hirsch et al (1982).

10. LIDAR: A TIME-OF-FLIGHT THOMSON BACKSCATTER DIAGNOSTIC

Thomson scattering from a wave packet whose spatial extent is short compared to the plasma dimensions has been proposed by Kristal (1978). The technique is pertinent to the study of plasma devices with plasma dimensions $\sim$ 1 metre and whose spatial temperature and density gradients are not too steep in terms of this scale length. Magnetic confinement configurations such as tokamaks for example produce appropriate plasmas with $T_e > 1$ keV, $n_e \simeq 10^{13} \rightarrow 10^{14}\ cm^{-3}$ and plasma dimensions typically in the range $0.5 \rightarrow 1$m. Using a visible probe beam in such an application, $\alpha << 1$ and the time variation of the scattered intensity $n_e S_e(k)$, integrated over the Gaussian frequency spread, is essentially the plasma density profile. The scattered light viewing optics has to be 'open' to the whole plasma diameter so that the background plasma light accepted is greater than is usual with Thomson scattering. Notwithstanding the short duration of the laser pulse, $\tau < 100$ ps, the requirement for a statistically significant number of scattered photons still means an appreciable energy in the incident laser pulse, $\sim$ 1 joule.

The resulting probe pulse intensity $> 1\ GW/cm^2$ gives a sufficiently high scattered light flux to discriminate easily against background

light. The unusually high intensity of the probe beam at the input window is something of a problem in short pulse scattering but any spurious light scatter from this surface can be discriminated against using the inherent time-of-flight differences between illumination of the optics and the plasma.

Time-of-flight light scattering becomes very attractive when considering plasma with dimensions in excess of 1 metre. Salzmann et al (1985) for example, propose to measure the electron parameters in the JET tokamak, whose minor plasma cross-section is 10 m^2, using time-of-flight Thomson backscatter or LIDAR (Light Detection and Ranging). The advantage of the backscatter geometry is that only a single (input) window is required in the plasma chamber. The scattered light collection optics and the probe beam focussing optics are in permanent alignment. Disadvantages of the 180° scattering geometry arise fom the large $\underline{\kappa}$ vectors sampled and the consequent wide spectral bandwidth of $S(\Omega,\kappa)$. A further drawback is the limited space resolution achievable using 'in-line' collection optics. In practice these factors prove to be appreciable, but not critical, design faults. Salzmann and Hirsch (1984) estimate that with $\tau_L \sim 300$ ps $E_L \sim 15$j (in the visible), then a space resolution $\Delta r < 10$ cm can be achieved in JET for $T_e(r)$, with a statistical error on the value of the T_e of the order or 10%. The spatial resolution is given by

$$\Delta r = \frac{c}{2(\tau_L + \tau_d)}$$

where τ_L is the laser pulse duration and τ_d the response time of the detection system.

Several laser systems have been considered such as frequency doubled IR and Ruby lasers. The range of possible detectors with subnanosecond response times, eg streak cameras, microchannel plate photomultipliers etc are discussed by Salzmann et al (1985).

11. SYNCHRONOUS MULTIPLE $\underline{\kappa}$ VECTOR SCATTERING FROM A PLASMA FOCUS

In this series of experiments Kirk (1984), Kirk et al (1982, 1983) the frequency spectrum of density fluctuations in a Plasma Focus device were investigated by Thomson scattering of ruby laser light. The co-operatively scattered ion feature $S_i(\underline{\kappa},\omega)$ were recorded simultaneously along different $\underline{\kappa}$ vectors, using an optical multichannel analyser, fig 15. This technique enabled density fluctuations associated with the current direction to be compared with those

orthogonal to the current flow. It also gave simultaneous $S(\underline{\kappa},\omega)$ spectra for different scattering parameters. The actual $\underline{\kappa}$ vectors selected and the scattering geometry are indicated in Fig 16.

The development of multiple $\underline{\kappa}$ scattering has an overwhelming advantage over the more usual single $\underline{\kappa}$ vector scattering when dealing with an irreproducible inhomogeneous plasma such as exists in the plasma focus. An example of the scattered spectra at different times during the discharge is shown in Fig 17.

Since the ion feature width is determined by $\Delta\omega = \kappa v_e$, the spectrum for $\underline{\kappa}_{45}°$ to the incident beam, with $\underline{\kappa} = 7 \times 10^4$ cm^{-1} is wider than its neighbours for $\underline{\kappa}_{10}°$ where $\underline{\kappa} = 1.6 \times 10^4$ cm^{-1}. It is evident also that the total intensity of the $\underline{\kappa}_{10}°$ spectra, $\underline{\kappa}$ directed along the electron current flow, are anomalously intense with respect to the (thermal) values of the intensity observed along the orthogonal $\underline{\kappa}$ vectors. The data is found to be most satisfactorily interpreted in terms of scattering from a double radial shell. The outer current-carrying thin shell scatters relatively little radiation but with a relatively high temperature and with superimposed electron drift, produces spectral shifts as indicated in Fig 18. The inner plasma core contributes the bulk of the scattered intensity with a spectrum which is characteristic of a relatively low temperature. At peak compression of the pinch onto the axis of symmetry, for example, the core plasma has, typically, electron and ion temperatures $T_e = 200$ eV and $T_i = 250$ eV respectively, while the outer current sheath region exhibits a shot-to-shot variation in the temperature structure with $T_e = 2.3$ keV; $T_i = 850$ eV and $T_e = 1.65$ keV; T_i 1.4 keV, respectively. An account of the detailed analysis is quite complex and is given by Kirk (1984). Here we only summarise the experimental results by stating that the relative enhancement and broadening of $S_i(\underline{\kappa},\omega)$ along the various $\underline{\kappa}$ vectors have been interpreted in terms of current driven turbulence. With the derived information on T_e, T_i, $\underline{v}_d$, $n_e S(\kappa)$, and the current distribution it has been possible to speculate on the mechanisms for induced turbulence. Lower-hybrid drift, electron cyclotron drift and ion acoustic instabilities are thought to play a role in the various phases of the discharge. Fig 18 gives an example of the analysis of the scattered spectrum in terms of the basic plasma parameters derived from an application of the scattering theory described earlier.

12. THOMSON SCATTERING FROM TURBULENCE IN LASER-PRODUCED PLASMAS ON A SUB NANOSECOND TIME-SCALE

Refraction and absorption make scattering with a probe beam frequency ω_0 close to the electron plasma frequency ω_{pe} unworkable in the presence of steep density gradients such as exist in laser produced plasmas from solid surfaces. Baldis and co-workers, at NRC Canada, in a series of studies, Baldis and Walsh (1981), (1982), (1983); Baldis et al (1982), Walsh et al (1982), Walsh and Baldis (1982); have cleverly exploited, therefore, the use of the second harmonic of a 1 μm Nd:YAG laser irradiation pulse to probe regions in the plasma expansion plume where the electron density has fallen to $n_e \lesssim 10^{19}$ cm^{-3}, Fig 19. The advantage of this arrangement is that non-linear wave coupling between a 10.6 μm pump CO_2 laser beam, Fig 20, and the plasma at a critical density surface can be observed directly in the scattered light spectrum. Minor changes in the scattering geometry and the polarisation of the pump field allow major differences in the electron and ion waves to be analysed with $\underline{\kappa}$ vectors in the 'p'-plane, ie., parallel to, or the 's'-plane, ie perpendicular to the electron density gradient.

Thomson scattering provides a unique signature of the many possible non-linear (and linear) coupling processes between the pump beam and the target plasma. These include Stimulated Brillouin Scattering (SBS), Walsh and Baldis (1982); Two Plasmon decay, Baldis and Walsh (1981) and Baldis and Walsh (1982); Stimulated Raman Scattering (SRS), Baldis and Walsh (1982), Parametric decay, and Resonance absorption, Walsh et al (1982).

It is not the purpose of this lecture to discuss in any detail the wave coupling physics which can be derived from these experiments. Suffice to say that identification of the coupling processes between the 10.6 μm pump beam and the plasma comes, in part, from the intensity of the co-operatively scattered light in $\underline{\kappa}$ space relative to the directions of the pump polarisation and of the plasma density gradient. The frequency shift of the electron waves $S_e(\omega,\kappa)$ and the ion feature broadening $S_i(\omega, \kappa)$ as illustrated in Fig 21, provide essential information on the wave spectrum. The time variation of the pump pulse and the appearance of the $S_e(\omega,\kappa)$ and $S_i(\omega,\kappa)$ features and the relation between the intensity of these features, and the pump power, also help to identify the wave coupling process, its threshold intensity and its saturation. Time resolution of the scattered spectrum of the order of 30 ps has been achieved, using an optical streak camera to record the scattered light spectrum while the duration

of the pump and probe beams can be adjusted by optical pulse clipping, Baldis et al (1982).

A time-resolved scattered light spectrum of the 2-plasmon decay instability is shown in Fig 22. The relevant plasma parameters and the scattering geometry are as indicated in Figures 19 and 20. The density surface where this particular interaction takes place is n_e (crit pump)/4 ie $\simeq 2.5 \times 10^{18}$ cm^{-3}. In figure 22 the far LHS 'monitor' shows the 80 ps modulation of the 0.53 μm probe beam with the neighbouring weaker signal proportional to the 10.6 μm pump intensity. Electron features shifted 125Å on either side of the central ion feature are seen to depend on the intensity of the pump beam and are modulated, of course, in step with the scattering probe ('monitor') illumination. At low pump intensities (at the top of the display) the ion feature is weak, with an intensity which is characteristic of thermal fluctuations. With increasing pump intensity (ie proceeding along the time axis, Fig 22,) the electron satellites become intense, $\sim 10^3 \rightarrow 10^4$ above the thermal level, indicating scattering from large amplitude electron plasma waves. The onset of enhanced ion fluctuations with an intensity dependent delay with respect to the electron wave is also seen, indicating a saturation of the electron wave amplitude, Baldis and Walsh (1981),(1982) and mode coupling to ion waves.

We have mentioned that the intensity of the scattered light in $\underline{\kappa}$ space is an important indication of the source mechanism which drives the plasma waves. In the case of non-linear coupling at density surfaces close to $n_{CRIT}/4$ there are several possibilities including 2 plasmon, SBS and SRS processes. The intensity thresholds, saturation levels and the intensity of the $S_e(\kappa,\omega)$ relative to $S_i(\omega,\kappa)$ will help to differentiate between these possibilities. A further important difference which is made use of in scattering experiments, Baldis and Walsh (1982), is the wavenumber of plasma waves, κ_ω, which show a maximum growth rate. For SBS the energy and wavenumber matching equations predict back-scattered ion acoustic waves with $|\underline{\kappa}_w| \sim |2|\underline{\kappa}_{pump}|$ and for SRS backscattered electron waves $|\underline{\kappa}_w| = (1 \rightarrow 2)|\underline{\kappa}_{pump}|$. The 2-plasmon process, on the other hand, generates waves at 45° to $\underline{\kappa}$ pump, and $|\underline{\kappa}_w| \simeq 6\,|\underline{\kappa}_{pump}|$. In setting up a 2-plasmon instability scattering experiment, the geometry is chosen so that $|\underline{\kappa}| \simeq \underline{\kappa}_w$, where $\frac{4\pi \sin(\theta/2)}{0.53\ \mu m} = |\underline{\kappa}| = 6\,|\underline{\kappa}_{pump}| = 6\,(\frac{2\pi}{10.6\ \mu m})$. A multiple $\underline{\kappa}$ vector scattering arrangement as shown in Fig 23, for example, allows a range of $\underline{\kappa}_w$, to be studied appropriate to scattering from the 2-plasmon instability. The spectral feature of interest, eg the electron feature, can be filtered by a spectrometer and streaked in time to give

the temporal $\underline{\kappa}$ space evolution of the instability. Baldis and co-workers, see eg Baldis and Walsh (1982), have very convincingly demonstrated the usefulness of these techniques.

13. RAMAN INDUCED KERR EFFECT (RIKE)

An interesting variation of Thomson scattering is the scattering from coherent electron density fluctuations driven by the ponderomotive potential which results from externally imposed pump waves. The technique is particularly applicable to the study of collective motions in a transient dense plasma. The intensity of the scattered wave in this non-linear wave mixing process is a function of the longitudinal dielectric constant and, as in ordinary Thomson scattering, contains information on the shape and intensity of the ion acoustic and plasmon resonances. The attraction of coherent multiple wave mixing is that the scattered wave is constrained to a narrow cone consistent with the wave vector matching and, as a consequence, the scattered power can be much enhanced over Thomson scattering for the free electron motion. Proposals for coherent four-wave scattering and for three wave scattering by the Raman Induced Kerr effect (RIKE) have been made by Praddaude et al (1979) and by Hellwarth (1976) respectively. Hellwarth, in the RIKE proposal, indicates that the scattered light enhancement over Thomson can be $\sim (\frac{\omega_0}{\omega_{pe}})^4$ for $\lambda_D < 0.1\,\lambda_0$. These schemes have not be yet been exploited as a practical scattering technique although studies of the scattered light from longitudinal plasma, waves, externally driven by lasers with frequencies ω_1 and ω_2 where $\omega_{pe} = \Delta\omega = |\omega_2 - \omega_1|$ and where the scattering vector $\underline{\kappa} = \Delta\underline{\kappa} = \underline{\kappa}_2 - \underline{\kappa}_1$ have been made, eg by Godfrey et al (1979); $\omega_2, \underline{\kappa}_2$ and $\omega_1, \underline{\kappa}_1$ define the imposed external beams. It is worthwhile noting the similarity of the technique with the work of Baldis and co-workers, section (12) where intensity thresholds for stimulating various instabilities were greatly exceeded with a single pump beam. In the present schemes for non-linear wave mixing the externally applied beam intensities are well below threshold for driving instabilities.

A schematic diagram comparing conventional Thomson scattering with the RIKE technique is shown in Fig 24. In the RIKE experiment the frequency difference between the probe and the pump beam approximate to ω_{pe} while the scattered wave is along the path of the $\Delta\omega$, broadband, transmitted probe beam. Use is made of the rotation of the scattered polarisation relative to that of the probe beam. The ratio of the RIKE signal recieved by the detector to the Thomson scattered signal for the same pump power has been caluculated by Goldman (1978) -

$$R = \frac{P_{RIKE}}{P_{INSC}} = \frac{n_e V}{64} \frac{\omega_{pe}}{\Delta\omega} \frac{(\omega_{pe})}{\gamma_L} \frac{1}{\alpha^2} \Lambda_B^2 \Lambda_0^2 \, |\hat{e}_B \cdot \hat{e}^*_0|^2 \qquad (19)$$

$\hat{e}_B$ and $\hat{e}_0$ are unit electric field vectors, see Fig (24); $n_e V$ is the number of plasma electrons included in the crossed pump and probe beam interaction region; $\frac{\omega_{pe}}{\gamma_L}$ is the effective Q of the Langmuir mode; Λ_B is the parameter which measures the non-linear effect and should be small if RIKE is to be a non-perturbing measurement; the symbols Λ_B, Λ_o represent the ratio of $\frac{\tilde{v}}{v_e}$, where $\tilde{v}$ is the jitter velocity of the electrons in the probe and pump fields respectively, $\Lambda = \frac{2\omega_{pe}^2}{\omega^2} \frac{\Phi}{m_e n_e c}$.

For $\alpha \simeq 10$ and collisional damping with $\frac{\gamma_c}{\omega_{pe}} \sim 2 \times 10^{-5}$ and for $\Phi = 3 \times 10^{11}$ w cm^{-2}, $\Lambda^2 = 10^{-4}$, $T_e = 1$ keV and $n_e = 10^{19}$ cm^{-3}; then the ratio R gives $\sim 10^6$.

The non-linear optical approach to scattering from ion or electron resonances in dense plasma appears therefore to be an attractive proposition.

ACKNOWLEDGEMENTS

The author would like to acknowledge the help and advice given by D E Evans and R E Kirk (Culham Laboratory), M Von Hellerman (JET), H Baldis (NRC) and M V Goldman (University of Colorado).

These lectures in modified form were first prepared for the NATO ASI Meeting on Fast Electrical and Optical Measurements at Castelvecchio Pascali, Italy (1983).

References

Baldis H. A., Walsh C J. and Benesch R., Applied Optics 21, 297-302 (1982).

Baldis H. A. and Walsh C. J., Phys. Rev. letts. 47 (23) 1658-1661, (1981).

Baldis H. A., and Walsh C. J., Physica Scripta, T2/2., 492-497 (1982).

Baldis H. A. and Walsh C. J., Phys Fluids 26 (5), 1375 (1983).

Bretz N., Dimock D., Foote V., Johnson D., Long D., and Tolnas E. Appl. Optics 17 192 (1978).

Carolan P. G., Plasma Physics 19, 757-775 (1977).

Evans D. E., Doyle E. J., Frigione D, Von Hellerman M, and Murdoch A. Plasma Phys. 25 (6) 617-640 (1983).

Evans D. E., Plasma Phys., 12, 573-584 (1970).

Evans D. E., In "Applied Atomic collision Physics" vol II - Controlled Thermonuclear Fusion. Chapt 6. publ. Academic Press (1984).

Evans D. E., and Katzenstein J., Rep. Prog. Phys. 32, 207-271 (1969).

Evans D. E., von Hellerman M., and Holzhauer E., Plasma Physics 24, (7), 819-834, (1982).

Fiocco G and Thompson E., Bull. Am Phys. Soc. [2], 8, 373, (1963a).

Fiocco G and Thompson E., Phys. Rev. Lett. 10, 89-91 (1963b).

Fried B. D and Conte S. D. 'The Plasma Dispersion Function' publ. Academic Press (1961).

Godfrey L. A., Nodwell R. A. and Curzon F. L. Phys. Rev. A. 20, (2) 567-577 (1979).

Goldman M. V., Private communication - University of Colorado (Boulder).

Hellwarth R. W., Appl. Phys. 11, 147-151, (1976).

Hirsch K. Rohr H., Salzmann H and Steuer K. H. University of Stuttgart report IPF-82-15 (1982). Also publ. Rev. Sc. Instr. (1983) Proc. 4th Topical Conference on High Temperature Plasma Diagnostics.

Kirk R. E., PhD. Thesis - University of London (1984).

Kirk R. E., Forrest M. J., Muir D. G., Peacock N. J., Proc. 3rd Int Workshop on Plasma Focus Research Stuttgart, IPF -83-6, 119-112. (1983).

Kirk R. E., Muir D G., Forrest M. J. and Peacock N. J. Proc. Int. Conf. on Plasma Phys. Goteburg-paper 14PI-03, (1982).

Kristal R., 'Diagnostics for Fusion Experiments' Proc. of Varenna School, (Editors - Sindoni and Wharton) p 617 (1978). Publ Pergamon Press.

Lehner G. and Pohl F., Zeit. Phys. 232, 405, (1970).

Muir D. PhD Thesis London University (1982).

Peacock N. J., 'Diagnostics for Fusion Experiments' - Proc of Varenna School, (Editors - Sindoni and Wharton), publ. Pergamon (1978).

Peacock N. J., Robinson D. C., Forrest M. J., Wilcock P. D., and Sannikov V. . Nature 224 488-490 (1969).

Pots B. F. M., Coumans J. J. H., and Schram D. C., Phys Fluids 24 (3) 517-527 (1981).

Praddaude H. C., Scudder D. W., and Lax B., Appl. Phys. Lett. 35, 766-768. (1979).

Rohr H., Steuer K. H., Scramm G., Hirsch K., and Salzmann H. Nuclear Fusion 22, 1099-1102 (1982).

Salzmann H. and Hirsch K., Rev., Sci. Instr. 55, 457, (1984).

Salzmann H., Hirsch K., Gruber J., Rohr H., Brederlow G., and Witte K. Rev Sc Inst 56 (5) 1030-1032 (1985).

Selden A. C., Phys. Letts. 79A, 405-406, (1980), Culham Laboratory Report. CLM-R220 (1982).

Sheffield J., "Plasma scattering of Electromagnetic Radiation" Academic Press Inc. (London) LTD. (1975).

Smith J., Chase R., Garcia J., Hsieh C., and Vaslow D. Rev Sc Inst 56 871, (1985).

Walsh C. J., and Baldis H. A., Phys. Rev Letts. 48, (21) 1483-1486 (1982).

Walsh C. J., Baldis H. A., and Evans R. G., Phys Fluids 25 (12) 2326-2333 (1982).

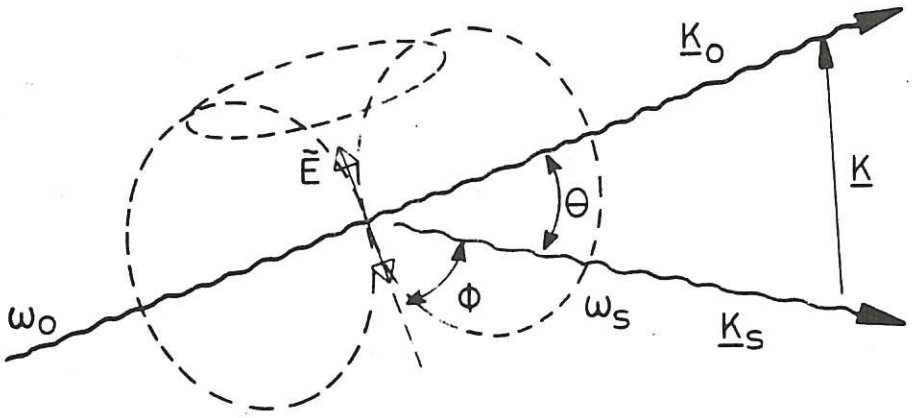

Fig. 1 Scattered dipole radiation from incident light beam with wave vector $\underline{\kappa}_0$ and polarisation vector $\tilde{E}$.

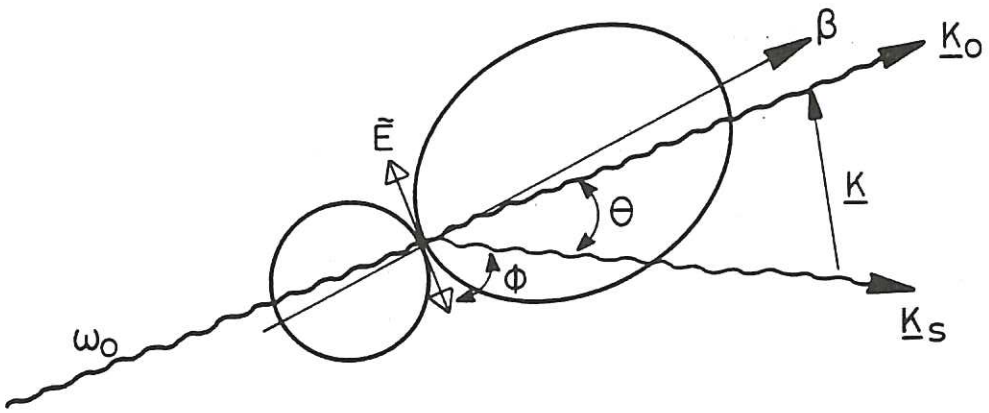

Fig. 2 Distorted dipole pattern of scattered radiation from relativistic electron with speed β .

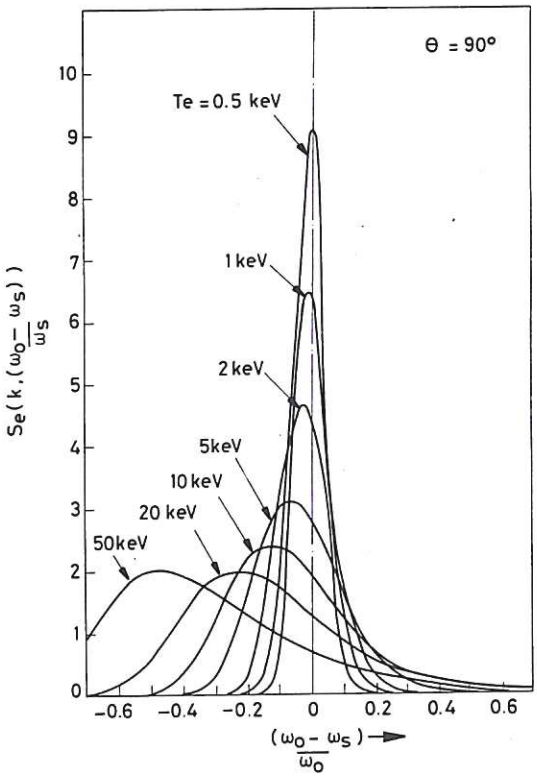

Fig. 3 Scattered light spectra from Maxwellian distributions of electrons. The spectra become progressively blue shifted and asymmetric as the distributions approach relativistic speeds. Selden (1982).

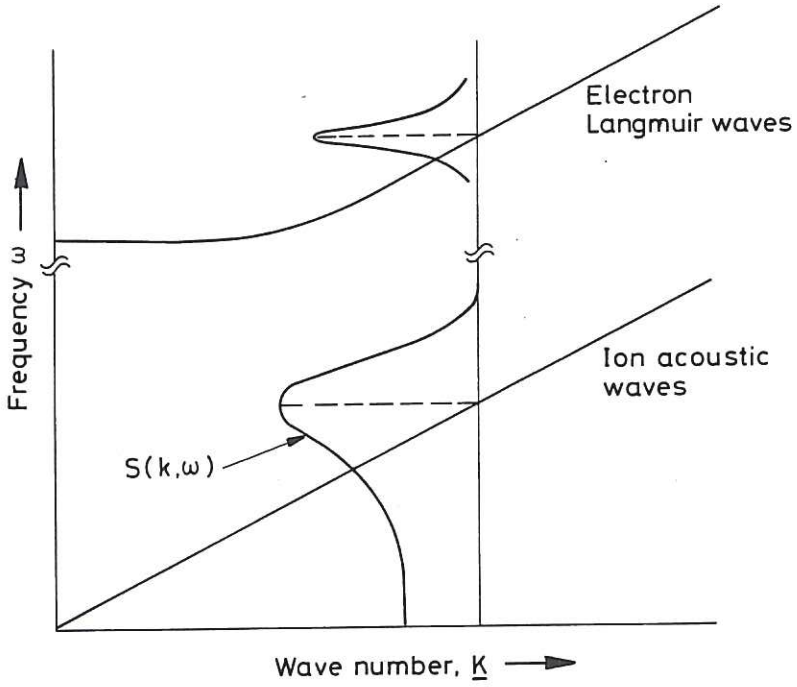

Fig. 4 Dispersion plot for plasma waves, see Fried and Conte (1961).

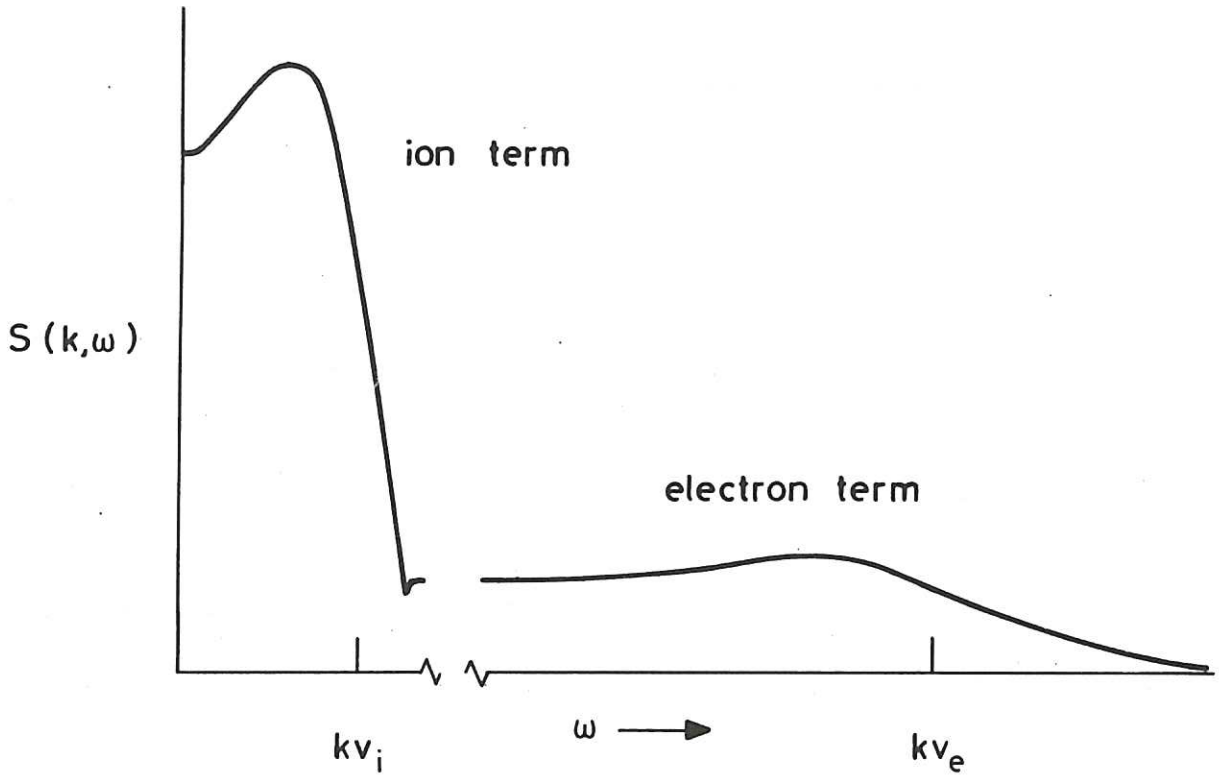

Fig. 5 Frequency spectrum of scattered radiation from a thermal plasma.

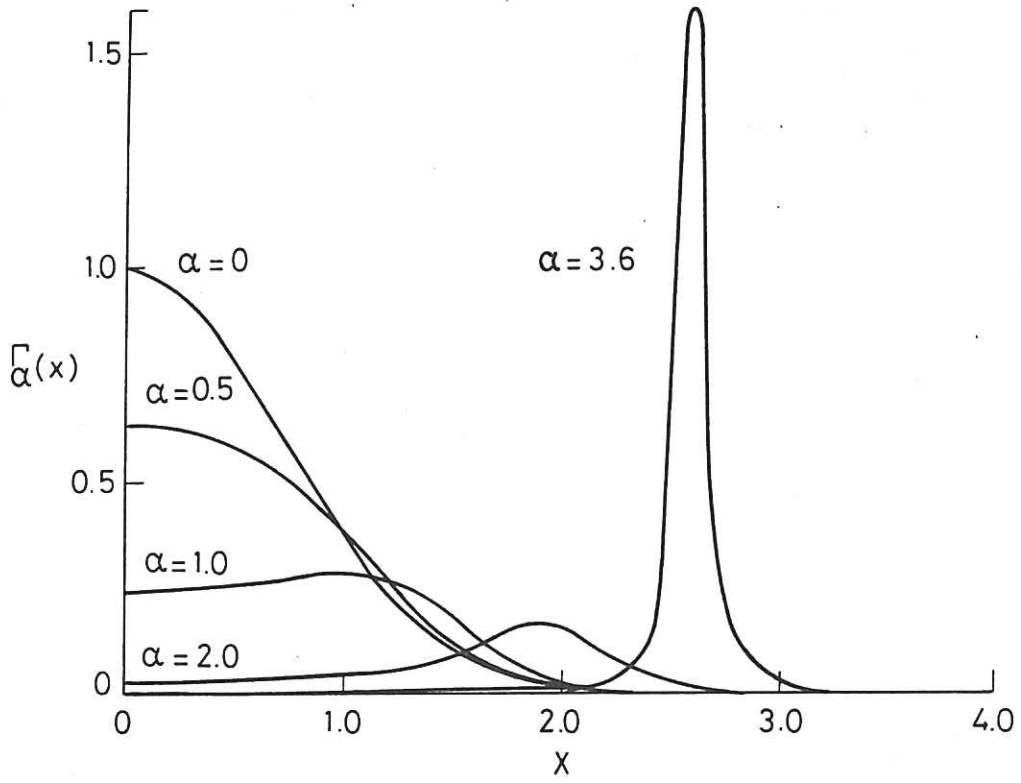

Fig. 6 Spectral distributions ($x = \Delta\omega/\kappa v_e$) of scattered light from electron fluctuations as a function of the scattering parameter 'α'. In this Saltpeter approximation the ion spectrum has a similar distribution with $\Gamma_\beta(x_i)$ and $x_i = \frac{\Delta\omega}{\kappa v_i}$

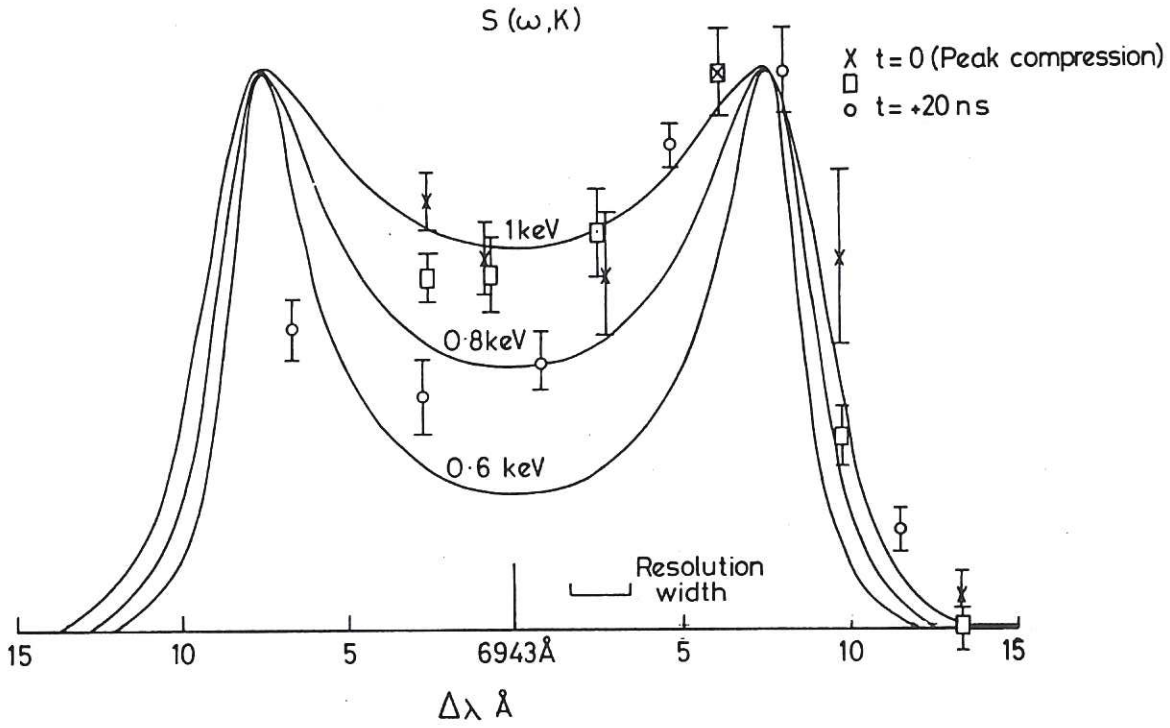

Fig. 7 Spectra, $S(\omega,\kappa)$ of co-operatively scattered ruby laser light viewed at 45° to the incident beam. The Plasma Focus filling pressure is 2.5 Torr D; 2+4% Ne; resolution width of the spectrometer is 1.8 Å. The double-humped form of $S(\omega,\kappa)$ is characteristic of the ratio $T_D/T_e<1$. The solid curves are calculated for deuterium ion temperatures, T_D, of 0.6, 0.8 and 1.0 keV, following Evans (1970).

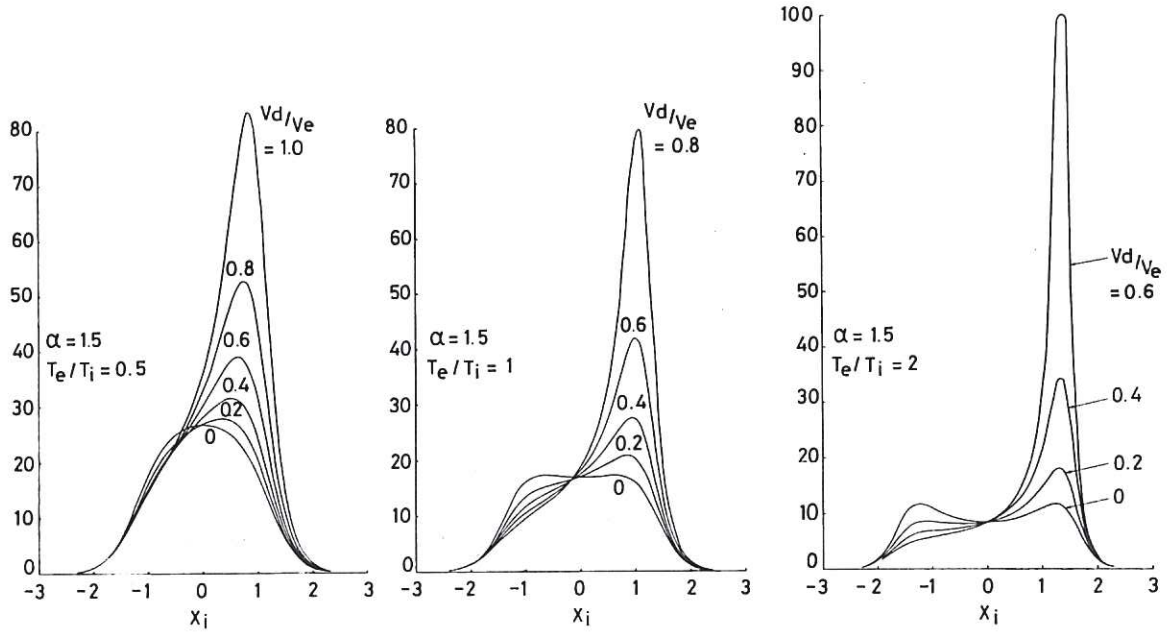

Fig. 8 Asymmetric ion spectra arising from electron drift V_d/V_e is the ratio of the electron drift velocity to their thermal speed, Evans and Katzenstein (1969).

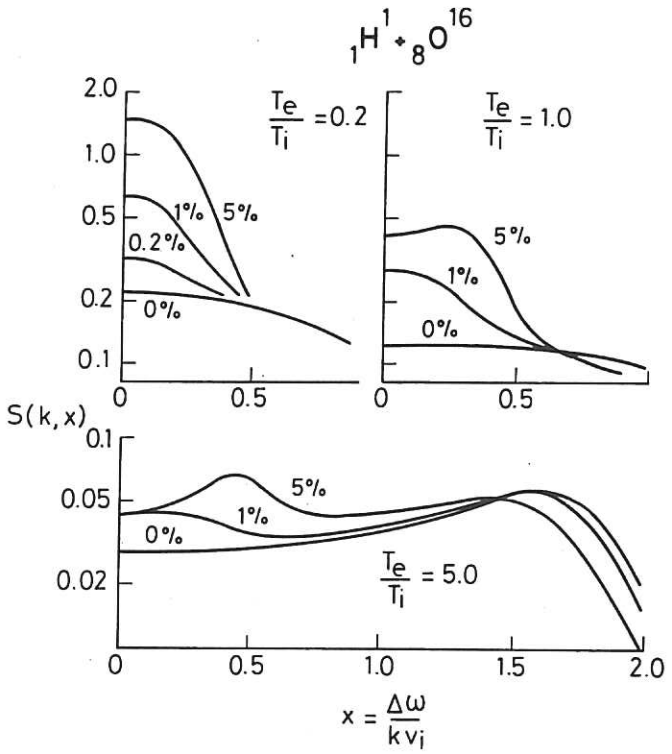

Fig. 9 Distortion to ion spectral density function due to presence of various fractions of oxygen nucleii in a hydrogen plasma. Evans (1970).

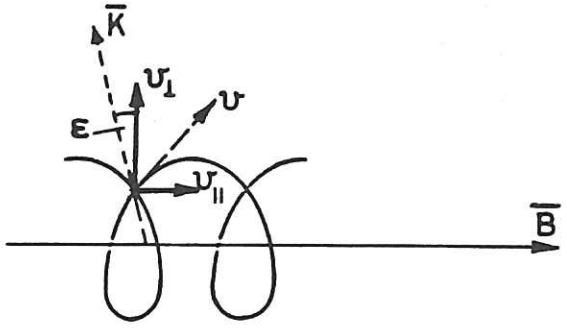

Fig. 10 Gyro-rotation of electron about magnetic field line $\bar{B}$. 'ϵ' is the misalignment angle between component of v perpendicular to $\bar{B}$ and the scattering vector $\varkappa$.

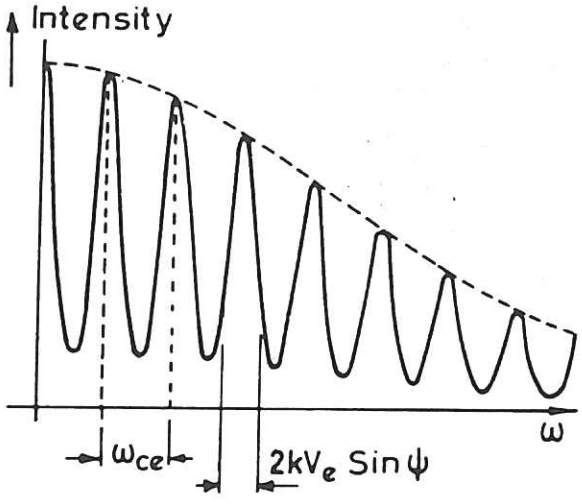

Fig. 11 Scattered spectrum from a magnetised plasma for $\varkappa$ perpendicular to $\bar{B}$.

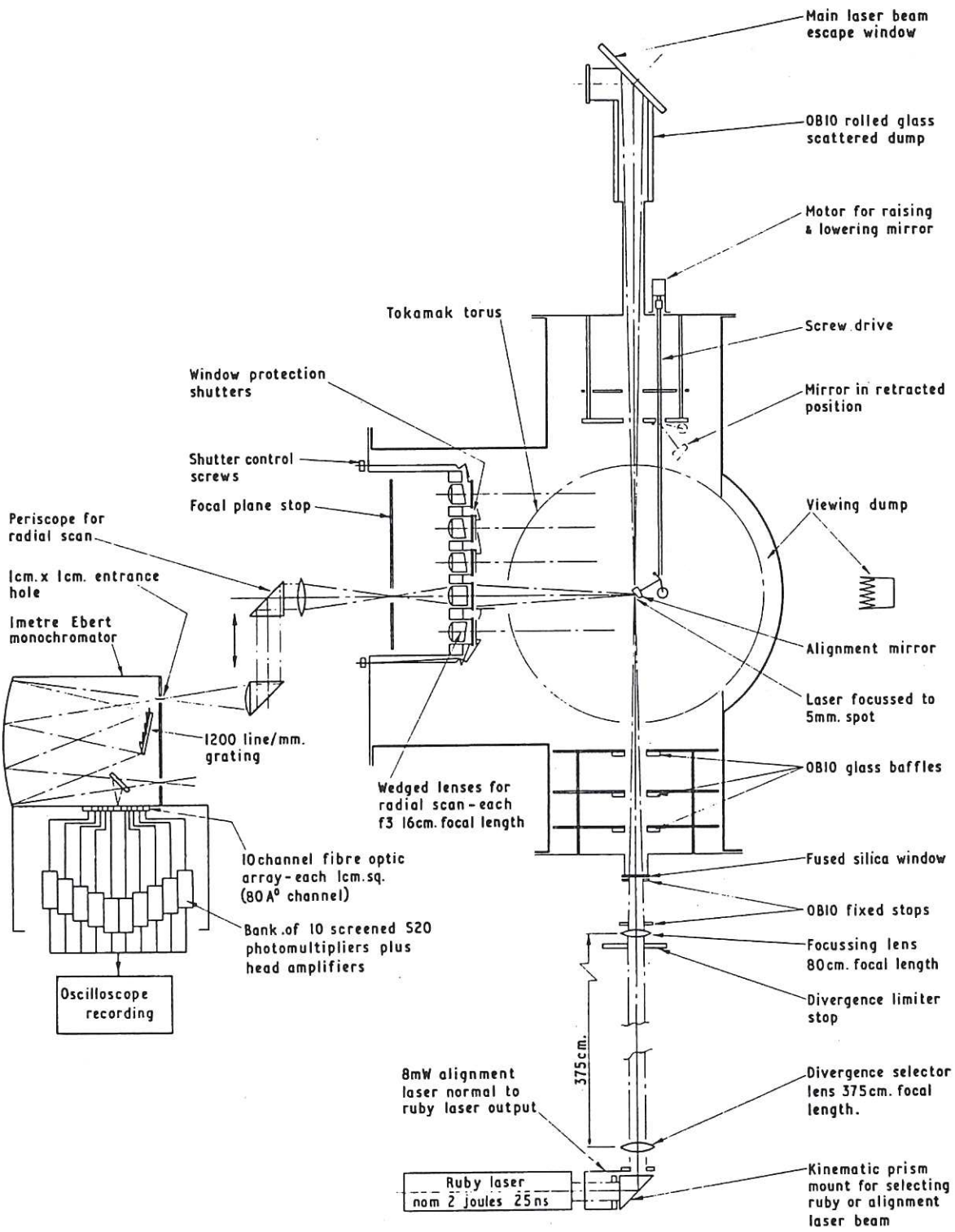

Fig. 12 Schematic diagram of the laser scattering experiment in tokamak T3-A. [Peacock et al (1969)].

Thomson scattering signals on axis, 20 msec from start of current

$\left[\hat{n}_e = 1{\cdot}7 \times 10^{13}\ ,\ B_0 = 25\ kG\ \ \hat{I}_z = 90\ kA\ ,\ \tau = 40\ msec\right]$

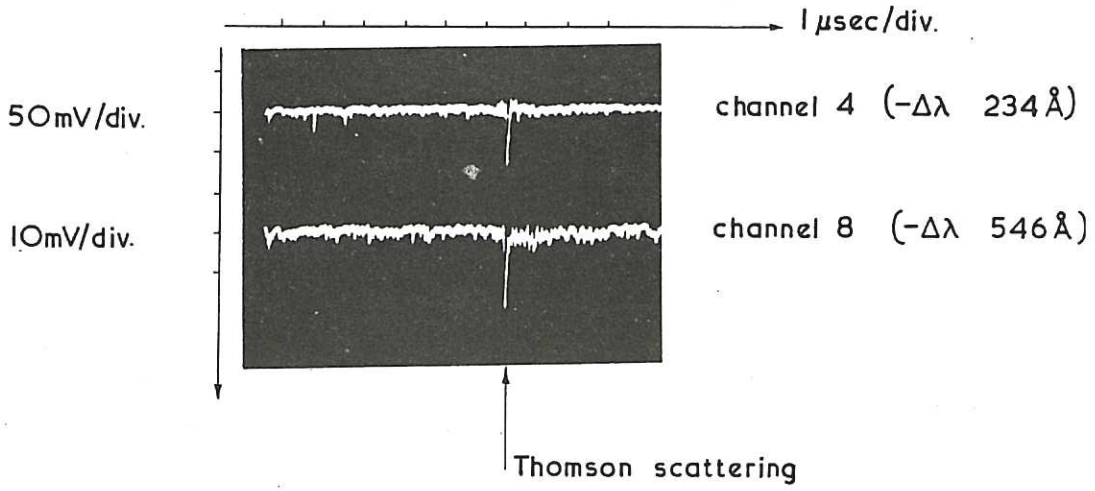

Fig. 13 Thomson scattering of Ruby laser light in two spectral channels 20ms from the start of the current pulse in the T3-A Tokamak.

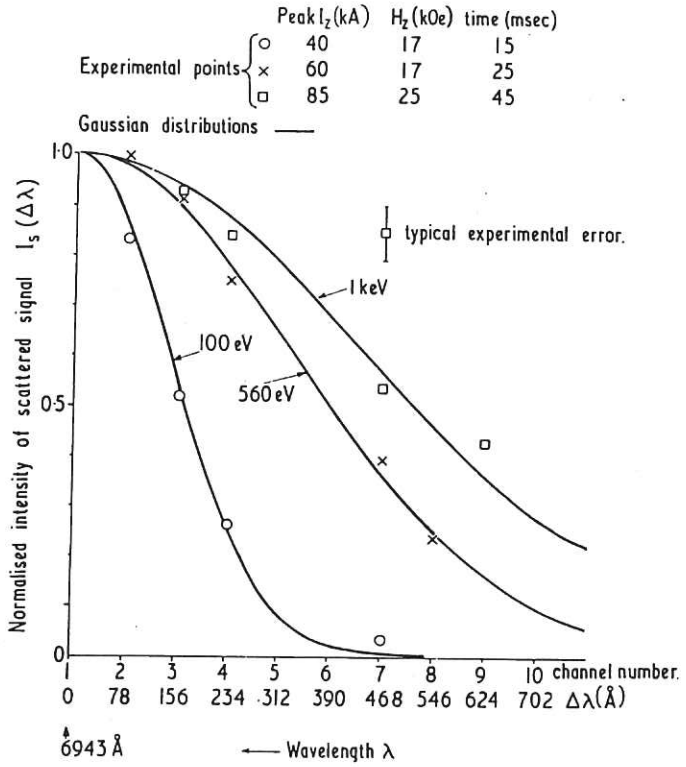

Fig. 14 Spectrum of scattered Ruby laser light from different plasma conditions in the T3-A tokamak.

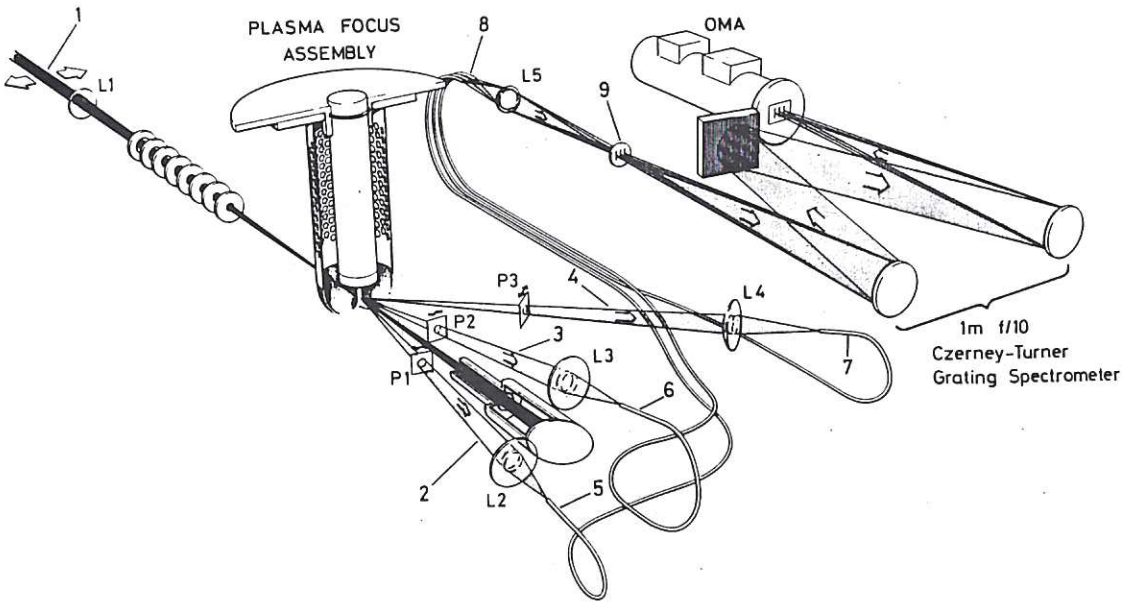

Fig. 15 Schematic of the optical layout of the multiple κ vector scattering experiment on Plasma Focus, Kirk (1984). The scattering light spectra from each of the separate κ vectors are recorded simultaneously by a multiple input slit spectrometer with OMA detector.

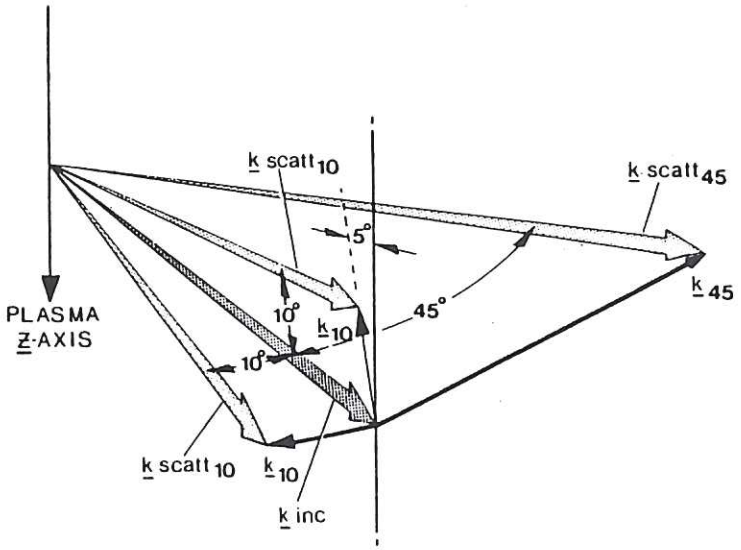

Fig. 16 Scattering vector diagram adopted for Plasma Focus experiments. Kirk (1984).

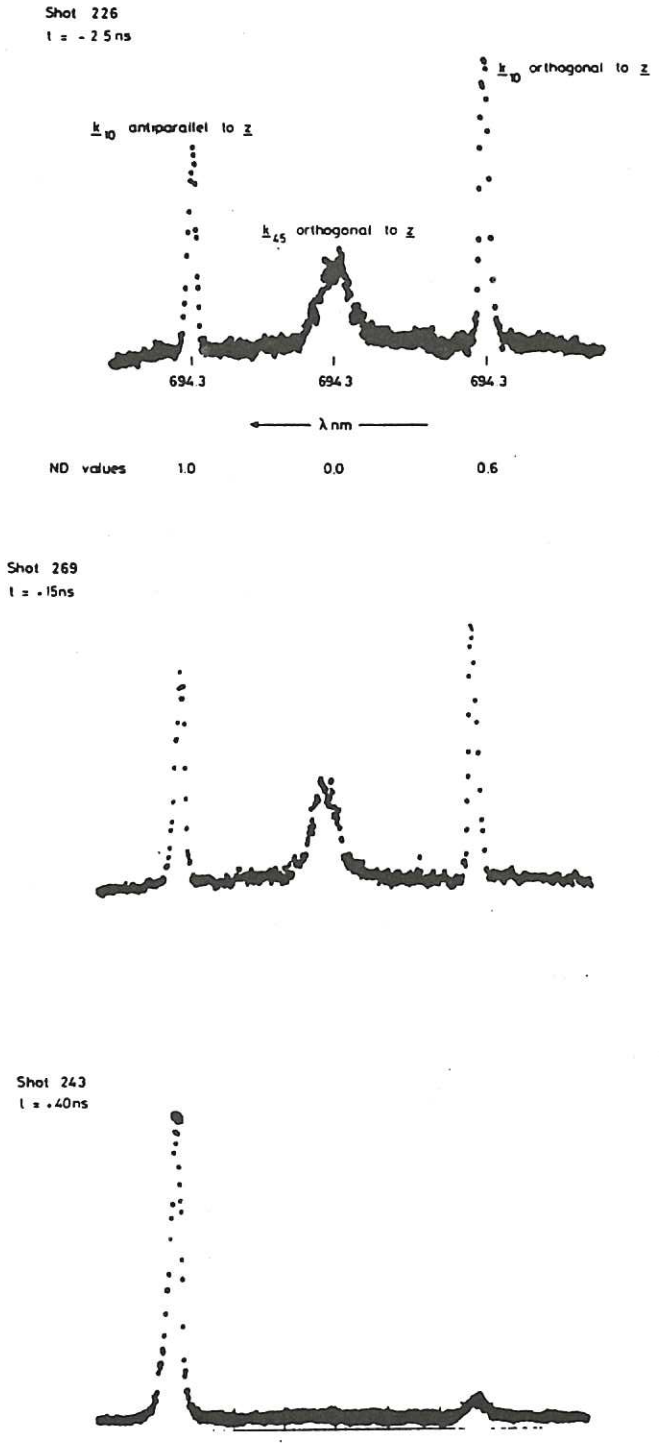

Fig. 17 Variation of the scattered light spectra, corresponding to different κ vectors, during the temporal evolution of the plasma in the plasma focus device, Kirk (1984). Note that, following peak plasma compression at t=0ns, the scattered light intensity, $n_e S(\kappa, \omega)$ for orthogonal κ vectors is much reduced compared to $\varkappa$ vectors parallel to the current flow.

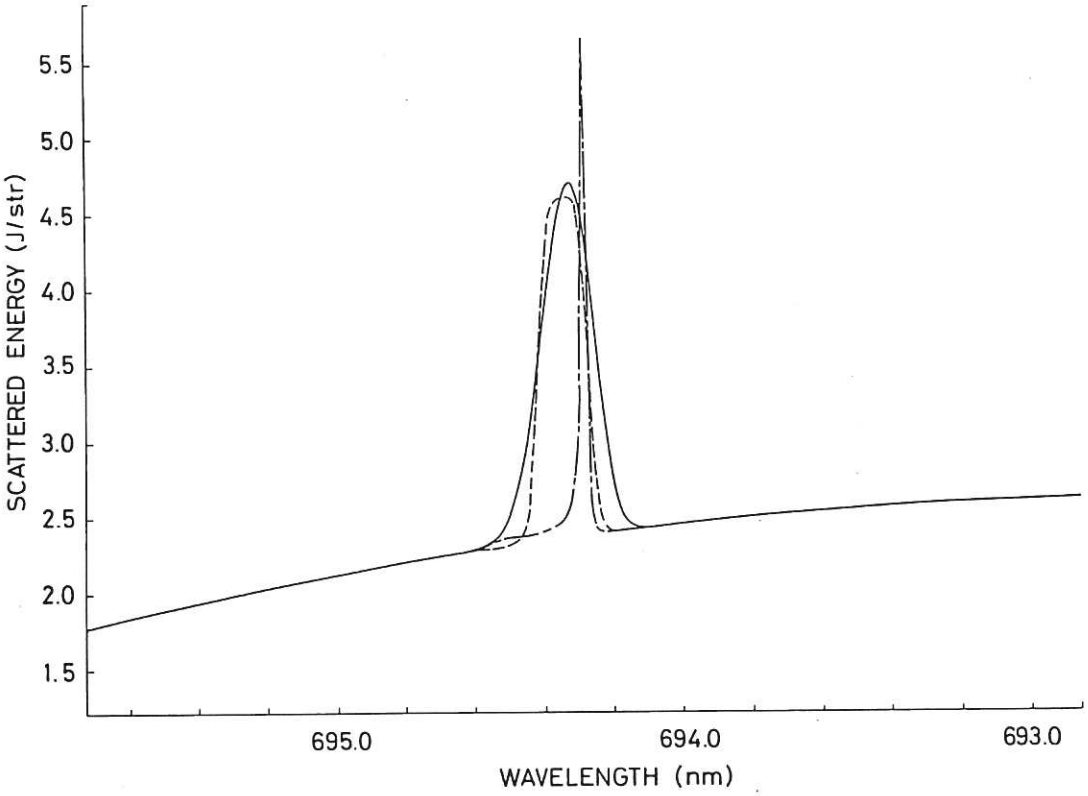

Fig. 18 Example of scattered light, spectrum, ———, at 0 ns for κ_{10° (anti-parallel). Analysis is based on two spatially separate fluids viz a relatively high temperature current sheath — — ($r_s = 2.5$ mm, $n_e = 2.4\times10^{18}$ cm^{-3}, $T_e = 967$ eV, $T_e = 350$ eV, $(\kappa\lambda_D)^{-1} = 4.3$, $v_r = 9\times10^6$ cm s^{-1}, $v_z = 3.5\times10^7$ cm s^{-1}) and a core region – – – – ($r_c = 1.1$ mm, $n_e = 7\times10^{18}$ cm^{-3}, $T_e = 107$ eV, $T_i = 182$ eV, $(\kappa\lambda_D)^{-1} = 23$, $v_r = 4\times10^6$ cm s^{-1}, $v_z = 2\times10^7$ cm s^{-1}). The contribution from the sheath region is blue-shifted with respect to the core region.

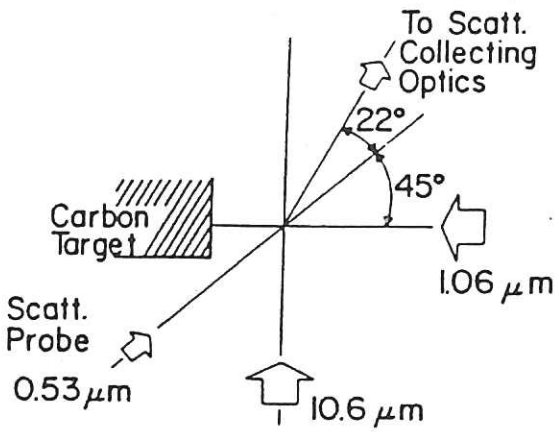

Fig. 19 Geometry of light scattering experiment on laser produced plasma, Baldis et al (1982). The wave vectors of the 0.53 μm probe beam, the scattered light, the 1.06 μm beam which generates the plasma and the 10.6 μm pump beam are all in the same plane.

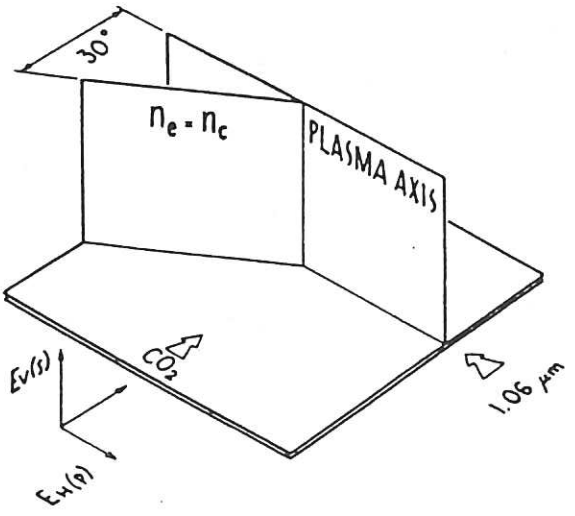

Fig. 20 Geometry for non-linear wave-coupling between 10.6 μm CO_2 pump laser and plasma waves at the critical density ($n_c \simeq 10^{19}$ cm^{-3}) surface in a laser produced plasma plume.

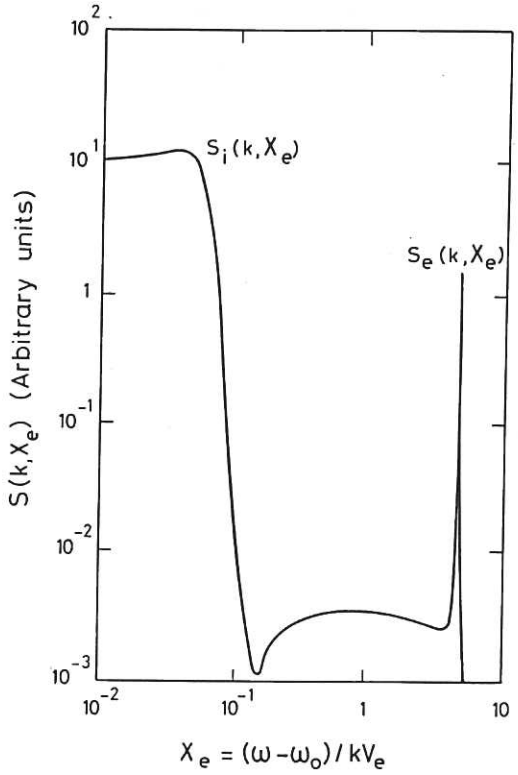

Fig. 21 Electron and ion components of the scattered light spectrum for $\alpha = 5$. ($T_e = 100$ eV and $n_e = 2.5 \times 10^{18}$ cm^{-3}). Baldis and Walsh (1983).

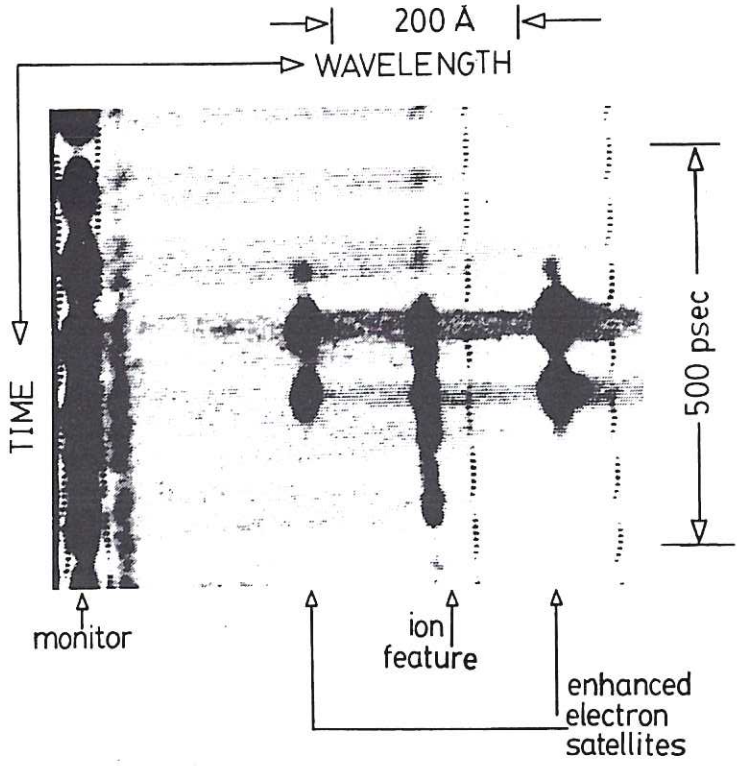

Fig. 22 Temporal evolution of non-thermal plasma fluctuations driven by 10.6 μm CO_2 pump laser. The LHS monitor signals shows the modulation of the probe beam. The scattered light from the electron and ion fluctuations (See Fig. 21) is in phase with the probe beam. The electron satellite features are $\gtrsim 10^3$ above thermal due to the 2-plasmon decay instability. The onset of the enhanced ion fluctuations has an intensity dependent delay with respect to the electron waves, Baldis et al (1982).

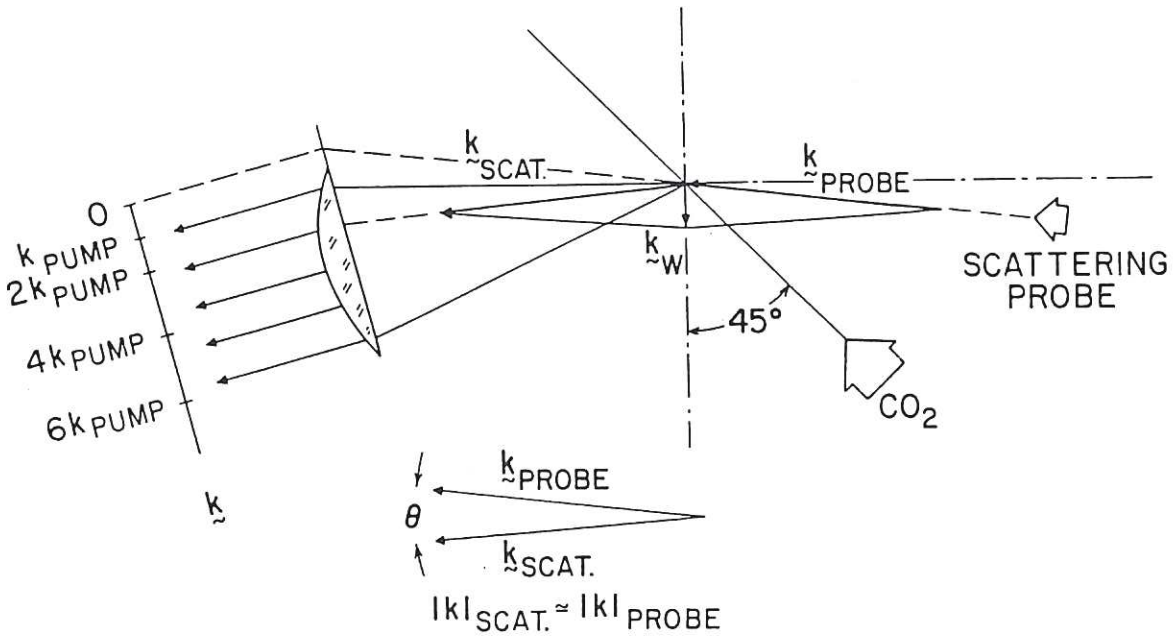

Fig. 23 Scattering geometry adopted for studying $\varkappa$ vector dependence on E_0 and κ_0 of pump wave. The distribution of light across the collection lens represents the intensity distribution in the range of κ space covered by the lens. Baldis and Walsh (1983).

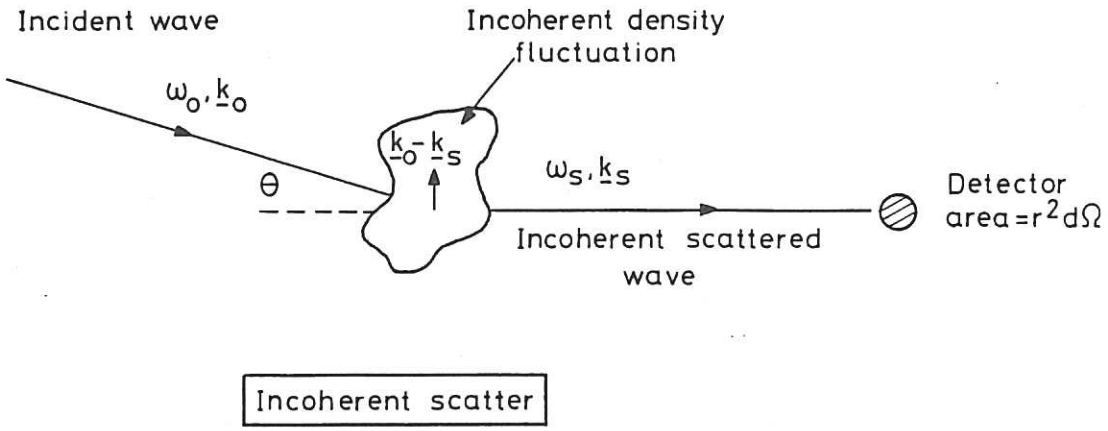

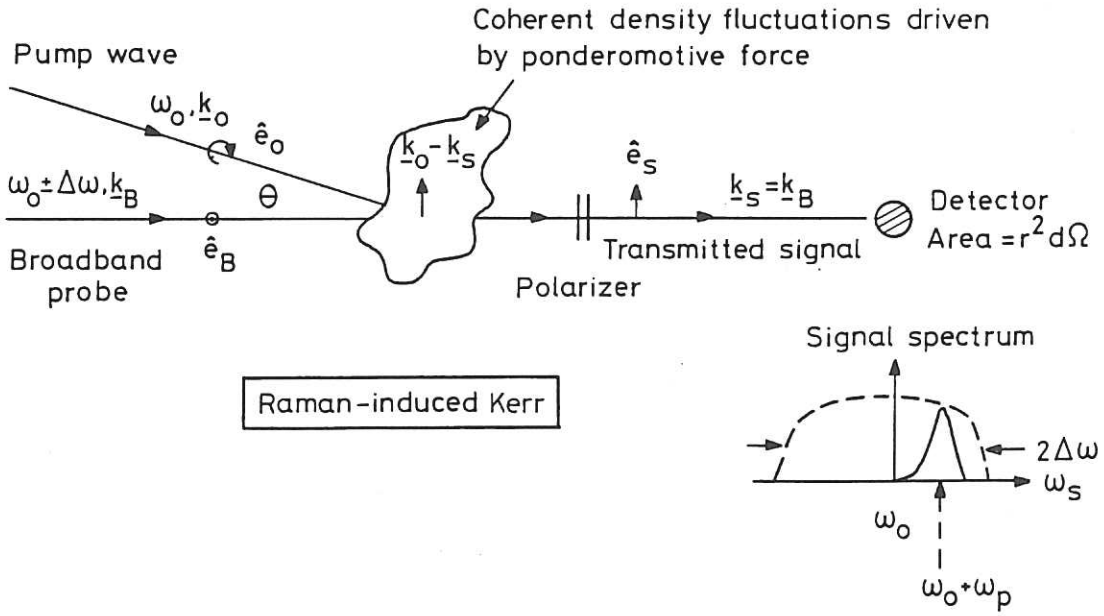

Fig. 24 Comparison of Raman Induced Kerr effect (RIKE) with the incoherent scatter (INSC) in a plasma.